Uniosun Journal of Engineering and Environmental Sciences (UJEES), Vol. 8 No. 2, Sept., 2026
DOI: 10.64980/ujees.v8i2.031 **Ojedokun et al.**
Published: September 30, 2026

OPTIMIZED LOAD FREQUENCY CONTROL OF A SOLAR PV-INTEGRATED TWO-AREA INTERCONNECTED POWER SYSTEM USING A HYBRID BROWN BEAR–GREY WOLF OPTIMIZATION ALGORITHM

Isaac A. OJEDOKUN[1], Olusola J. OYEDELE[2*], Oluwadare A. ADEBISI[3], Babajide T. OSONUGA[4], Ademola R. ADETELA[5], Titilola T. OLAYINKA[6], Olubunmi F. ATILOLA[7]

[1,2,3,4,5]Department of Electrical and Electronic Engineering, Bowen University Iwo, Osun State Nigeria

[6]Department of Electrical and Electronic Engineering, Ajayi Crowther University, Oyo, Oyo State, Nigeria

[7]Department of Electrical and Electronic Engineering, Redeemer's University, Ede, Osun State, Nigeria

[*]Corresponding Author: olusola.oyedele@bowen.edu.ng

Abstract
Higher solar PV penetration poses frequency regulation issues since inverter-interfaced PV generation offers minimal inherent inertia and governor response, while fast variations of PV add another disturbance to the grid. In this study, a two-stage LFC scheme for a two-area power system with PV integration is designed, differentiating optimization issues from controller structure issues. In the first stage, an area control error-based PID controller is designed using Hybrid Brown Bear-Grey Wolf Optimization (BBO-GWO) and is compared against Brown Bear Optimization, Political Optimizer, Grey Wolf Optimization, particle swarm optimization, and genetic algorithm. Thirty independent optimization runs, Wilcoxon test, and parameter variation analysis are carried out to evaluate the consistency and robustness of the optimization. In the second stage, the optimized PID is compared against a two-degree-of-freedom PID (2DOF-PID) and a PV-aware 2DOF-PID controller, which takes the measured PV active power as an additional feedforward signal. Using Hybrid BBO-GWO, Area 1 ITAE is reduced by 95.2%, settling time is reduced from 8.26 to 2.34 s relative to trial-and-error PID, and stability under ±20% parameter variation is achieved. While the optimization performance is statistically equivalent to other algorithms, the controller structure gives a higher gain in terms of frequency regulation under PV fluctuation. The hybridization of BBO-GWO–PV awareness based 2DOF-PID controller shows that effective tuning and the use of measured PV-power feedforward significantly enhance frequency regulation in the presence of load and renewables disturbances; it is advisable for future studies to verify the effectiveness of the developed framework on real power system networks.

Keywords
2DOF-PID, Brown Bear Optimisation, feedforward control, Grey Wolf Optimisation,, load frequency control, solar PV integration, two-area power system

1. INTRODUCTION

Load frequency control (LFC) keeps the system frequency within permissible limits and regulates the tie-line power flows between control areas after a load–generation imbalance [1], [2]. The two-area system is the standard test case for LFC studies: the generating units in each area are coupled through a tie-line, so an imbalance in one area produces a frequency deviation in that area and a corresponding deviation in the other. The LFC objective is achieved by modulating the governor set-points in response to the frequency and tie-line power deviations, using primary speed-droop control together with a secondary proportional–integral–derivative (PID) controller acting on the area control error (ACE) [3].

Solar photovoltaic (PV) generation creates two specific difficulties for LFC. First, the inverter interface contributes no rotational inertia, so the rate and depth of frequency excursions increase as PV displaces synchronous generation [4], [5]. Second, PV output follows solar irradiance rather than load demand, so passing clouds inject fast power fluctuations that act as an additional, largely unscheduled disturbance [6]. These difficulties are of practical interest in Nigeria, whose 330 kV national grid has experienced repeated system collapses [7], which makes robust frequency regulation a practical concern. The present study, however, uses a generic two-area benchmark rather than a model of the Nigerian grid; the characteristics of the Nigerian system that the benchmark does and does not represent are set out in Section III-C, and the conclusions are stated accordingly.

Conventional PID design methods, such as trial-and-error, Ziegler–Nichols and pole placement, are simple to apply but give limited performance when the plant is disturbed by variable renewable generation [8], [9]. Metaheuristic optimisation can search the controller parameter space directly against a time-domain performance index, but each algorithm has its own balance between exploration and exploitation, and no single algorithm is best for every problem [10]. This paper uses Brown Bear Optimisation (BBO), which is inspired by the scent-marking and sniffing behaviour of brown bears [11], and the Political Optimiser (POA), which models multi-party political behaviour [12], and proposes a hybrid algorithm (Hybrid BBO-GWO) that combines the exploratory moves of BBO with the leader-guided exploitation of Grey Wolf Optimisation (GWO) [13], benchmarking it against GWO, particle swarm optimisation (PSO) and a genetic algorithm (GA) as well as its parent algorithms.

Beyond tuning, the controller structure determines which disturbances the controller can observe. A feedback-only PID can act only after the frequency has deviated, whereas a feedforward path can act as soon as a disturbance is measured. Separating the benefit of better tuning from the benefit of a better structure is therefore the central question of this paper. The main contributions are as follows:

i. A unified two-stage evaluation framework in which the same two-area plant, ITAE objective and optimiser are used throughout: Stage I compares tuning algorithms for a fixed PID structure, and Stage II compares controller structures for a fixed tuning algorithm, so that the gains from tuning and from structure can be separated.
ii. A Hybrid BBO-GWO tuning algorithm, fully specified in Section III-H4, which switches probabilistically between BBO exploration and GWO leader-guided exploitation, benchmarked against BBO, POA, GWO, PSO and GA over 30 independent runs with Wilcoxon rank-sum tests and ±10–20% robustness tests. The hybrid removes the premature stagnation of BBO (30 of 30 successful runs instead of 0 of 30) and matches GWO, while PSO and GA perform marginally better on this problem.
iii. A PV-aware 2DOF-PID controller (2DOF-PID-PV) that adds measured PV active power as a second feedforward channel and reduces the ITAE of a PV cloud transient by 78.8%, whereas load-only feedforward gives no improvement (+0.1%).
iv. A design guideline supported by the results: for a PV-integrated system, extending what the controller measures yields larger improvements than changing the metaheuristic used to tune it. The primary contribution of the paper is therefore the PV-aware control structure evaluated within the unified framework; the hybrid optimiser is the enabling tuning tool.

The rest of the paper is organised as follows. Section II reviews related work and states the research gap. Section III presents the system model, controller structures, disturbance scenarios, objective functions and optimisation algorithms. Section IV presents and discusses the Stage I and Stage II results and the limitations of the study, and Section V concludes the paper.

The ACE concept, which combines the frequency deviation and the tie-line power deviation of an area into a single control signal, was formalised in classical treatments of LFC [1], [2], and the control framework was later extended to robust and multi-objective designs [3]. Surveys of automatic generation control (AGC) have traced the development of LFC from classical integral and PI/PID control to optimal, adaptive, robust and intelligent schemes [14], [15], including LFC in deregulated environments [16]. More recent reviews emphasise the effects of renewable energy sources, electric vehicles, energy storage and communication constraints on LFC [17], as well as data-driven and cyber-resilient strategies and the importance of reporting practical non-linearities such as governor dead-band and generation rate constraints [18].

The loss of rotational inertia as converter-interfaced generation increases has been identified as a key threat to frequency stability, since it raises the rate of change of frequency and deepens the frequency nadir after a disturbance [4], [5]. For PV in particular, one-second measurements at large plants have shown that passing clouds can change plant output by a large fraction of its rating within seconds to tens of seconds [6]. In LFC studies, Moghaddam et al. [19] showed that a fuzzy-PID controller outperforms a conventional PID in a two-area system with renewable sources. In most such studies, however, renewable variability is treated as an unmeasured disturbance that the feedback controller must correct after it has affected the frequency.

PID-type controllers remain the most widely used LFC structure because of their simplicity [9], and analytical tuning methods such as internal model control have been proposed for them [8]. Metaheuristic tuning has received considerable attention because it handles non-convex, simulation-based objective functions without requiring gradient information. Early approaches include genetic algorithms (GA) [20] and particle swarm optimisation (PSO) [21]. GWO [13] has been applied to LFC of interconnected systems with good results [22], and Orka et al. [23] reported faster convergence and improved frequency regulation using an enhanced gradient-based optimiser for a two-area system. Wazir et al. [24] compared several optimisation algorithms for integral controller design in multi-area interconnected grids. BBO [11] and POA [12] are recent algorithms whose use in LFC remains limited; BBO was applied to integral-controller design in [24].

Because no algorithm is best for all problems [10], hybrids that combine a strongly exploratory algorithm with a strongly exploitative one are a common way to make the search more reliable.
Controller structure has also been extended beyond one degree of freedom. Sahu et al. [25] showed that a differential-evolution-optimised parallel 2DOF-PID controller outperforms a conventional PID in the presence of governor dead-band, and Shahi et al. [26] proposed a hybrid 2DOF-PID and tilt-derivative (2DOF-PID-TD) controller for an interconnected thermal–hydro system. Feedforward compensation of measured disturbances within AGC has also been discussed in the robust frequency control literature [3]. These 2DOF designs, however, generally shape the response to the reference or to the load disturbance and do not use renewable generation telemetry as a separate feedforward input.
Three gaps follow from this review. (i) Most studies evaluate either a new tuning algorithm for a fixed controller or a new controller structure with a single tuning method, so the relative contributions of tuning and structure to the final performance cannot be separated. (ii) Where PV is included, its fluctuations are usually treated as an unmeasured disturbance, and the use of measured PV power as a feedforward signal in two-area LFC has received little attention. (iii) BBO and POA have seen limited application to LFC and, to the best of the authors' knowledge, a BBO-GWO hybrid has not been reported for this problem. This paper addresses these gaps through the two-stage framework described in Section III, evaluated with several error-integral and time-domain metrics rather than a single performance index.

2. MATERIALS AND METHOD

2.1 Overall Framework

The study follows a two-stage framework built on a single two-area plant model and a single objective function. Stage I (tuning comparison) holds the controller structure fixed as a feedback PID acting on the ACE and compares a trial-and-error PID with PID controllers tuned by BBO, POA, GWO, PSO, GA and Hybrid BBO-GWO under step load perturbations (SLPs), including a 30-run statistical comparison and robustness tests. Stage II (structure comparison and validation) holds the tuning algorithm fixed as Hybrid BBO-GWO and compares three controller structures, namely the feedback-only PID, the 2DOF-PID and the 2DOF-PID-PV, under a combined SLP and PV cloud-transient disturbance. Both stages use the linear model of Section III-B implemented in MATLAB. Stage I uses the exact modal (eigenvalue) solution of the closed-loop state-space model, which makes the thousands of fitness evaluations required by the statistical study fast and free of integration error. Stage II uses ode45 because the PV disturbance is time-varying, and the Stage II model was also implemented independently in Python (SciPy solve_ivp) to confirm that the results do not depend on the solver. As a consistency check, the Stage I implementation reproduces the Stage II feedback-only PID load-step results exactly (ITAE 0.0857, ISE 0.00197 and frequency nadir 49.9158 Hz; Table IX).

2.2 System and Component Modelling

Each area consists of a speed governor (G_g), a non-reheat turbine (G_t) and a generator–load block (G_{ps}), and the two areas are connected by a tie-line. A PV plant is connected in Area 1 through an inverter and contributes to the area power balance without inertia or droop. The transfer functions of the governor, turbine and generator–load blocks are:

$$G_g(s) = \frac{1}{1+sT_g} \quad (1)$$

$$G_t(s) = \frac{1}{1+sT_t} \quad (2)$$

$$G_{ps}(s) = \frac{K_{ps}}{1+sT_{ps}}, \qquad K_{ps} = \frac{1}{D}, \qquad T_{ps} = \frac{2H}{f_0 D} \quad (3)$$

where T_g and T_t are the governor and turbine time constants (s), K_{ps} is the power-system gain (Hz/p.u. MW), T_{ps} is the power-system time constant (s), H is the inertia constant (s), f_0 is the nominal frequency (Hz) and D is the load-damping coefficient (p.u. MW/Hz). The governor, turbine and power balance of area k ($k = 1,2$) are then described by:

$$\Delta P_{g,k}(s) = G_g(s)\left[\Delta P_{c,k}(s) - \frac{1}{R_k}\Delta f_k(s)\right] \quad (4)$$

$$\Delta P_{m,k}(s) = G_t(s)\,\Delta P_{g,k}(s) \quad (5)$$

$$\Delta f_k(s) = G_{ps}(s)\left[\Delta P_{m,k}(s) + \Delta P_{PV,k}(s) - \Delta P_{L,k}(s) - a_k\,\Delta P_{tie,12}(s)\right] \quad (6)$$

where $\Delta P_{c,k}$ is the secondary control signal, $\Delta P_{g,k}$ is the governor output, $\Delta P_{m,k}$ is the turbine mechanical power, $\Delta P_{L,k}$ is the load disturbance, $\Delta P_{PV,k}$ is the PV power deviation ($\Delta P_{PV,2} = 0$ because the PV plant is in Area 1), R_k is the speed regulation (Hz/p.u. MW), and $a_1 = 1$, $a_2 = a_{12} = -1$ for areas of equal rating. All power quantities are in per unit on the area base.

Sign conventions. A positive Δf_k denotes a frequency above nominal. A positive $\Delta P_{L,k}$ denotes a load increase, so a positive SLP causes a frequency decline. Positive $\Delta P_{m,k}$ and $\Delta P_{PV,k}$ denote increases in conventional and PV generation, so a cloud-induced reduction in PV output is negative. A positive $\Delta P_{tie,12}$ denotes an increase in the power exported from Area 1 to Area 2.

The tie-line power deviation is driven by the difference between the two area frequencies through the synchronising coefficient T_{12}:

$$\Delta P_{tie,12}(s) = \frac{2\pi T_{12}}{s}[\Delta f_1(s) - \Delta f_2(s)] \quad (7)$$

The input to the secondary controller of each area is its ACE, given by Eqs. (8) and (9):

$$ACE_1 = B_1 \Delta f_1 + \Delta P_{tie,12} \quad (8)$$

$$ACE_2 = B_2 \Delta f_2 + a_{12}\Delta P_{tie,12} = B_2 \Delta f_2 - \Delta P_{tie,12} \quad (9)$$

where B_k is the frequency-bias factor of area k, set equal to the area frequency response characteristic:

$$B_k = D_k + \frac{1}{R_k} \quad (10)$$

In Stage I, the secondary controller of each area is a PID controller with the control law:

$$\Delta P_{c,k}(t) = -\left[k_{p,k} ACE_k(t) + k_{i,k}\int_0^t A\,CE_k(\tau)\,d\tau + \quad k_{d,k}\frac{dACE_k(t)}{dt}\right] \quad (11)$$

where $k_{p,k}$, $k_{i,k}$ and $k_{d,k}$ are the proportional, integral and derivative gains of area k. The negative sign ensures that a negative ACE (a generation deficit) raises the governor set-point. The plant parameters, their units and their physical meaning are listed in Table 1.

Table 1: Model, disturbance and optimisation parameters

Parameter (physical meaning)	Symbol	Value	Unit
Nominal frequency	f_0	50	Hz
Area rating (per-unit base; all powers in p.u. of this rating)	P_r	1.0	p.u.
Governor time constant	T_g	0.08	s
Turbine time constant (non-reheat)	T_t	0.3	s
Power-system gain, 1/D	K_{ps}	120	Hz/p.u. MW
Power-system time constant	T_{ps}	20	s
Load-damping coefficient (load change per unit frequency change)	D	0.00833	p.u. MW/Hz
Inertia constant (stored kinetic energy per unit rating)	H	4.17	s
Speed regulation (droop)	R	2.4	Hz/p.u. MW
Frequency-bias factor, D + 1/R	B	0.425	p.u. MW/Hz
Tie-line synchronising coefficient	T_{12}	0.0866	p.u. MW/rad
Area size ratio	a_{12}	−1	–
PV plant, modelled as an active-power injection in Area 1	$\Delta P_{PV,1}$	0 (Stage I); profile of Eq. (14) (Stage II)	p.u.
Step load perturbation	$\Delta P_{L,k}$	0.1; 0.5	p.u.
Derivative filter time constant	T_f	0.05	s
PID gain bounds	k_p, k_i, k_d	[0, 5]; [0, 5]; [0, 1]	–

Parameter (physical meaning)	Symbol	Value	Unit
Trial-and-error PID gains (both areas)	k_p, k_i, k_d	0.5; 0.5; 0.1	–
Population / iterations / runs (Stage I)	–	30 / 100 / 30	–
Population / iterations (Stage II)	–	16 / 30	–
Hybrid switching probability	P	0.5	–
Simulation horizon / output step (Stage I)	T	20 / 0.01	s

2.3 Scope of the Model and Relevance to the Nigerian Grid

The model is a representative two-area benchmark with standard non-reheat thermal parameters [1], [3], used here with a nominal frequency of 50 Hz. It is not a validated model of the Nigerian interconnected system. It represents the features of the Nigerian grid that are relevant to the question studied: a 50 Hz synchronous system, interconnected areas exchanging power over tie-lines, secondary frequency control through the ACE, and PV generation that contributes no inertia. It does not represent the actual Nigerian generation mix, which is dominated by gas-fired thermal and hydro units, the topology and impedances of the 330 kV network, measured inertia and damping, governor dead-band, generation rate constraints, communication delays, or measured PV irradiance data. The numerical results should therefore be read as evidence about the relative merit of tuning methods and controller structures on a benchmark system, not as predictions of the behaviour of the Nigerian grid.

2.4 Controller Structures for Stage II

Stage II compares three controller structures. The feedback-only PID is Eq. (11) implemented with a first-order derivative filter of time constant $T_f = 0.05$ s, which makes the derivative action realisable for step inputs. Because the reference in a frequency-regulation task is zero, the set-point-weighting form of a 2DOF-PID has no effect; the second degree of freedom is therefore obtained with a disturbance feedforward path, as in feedforward-augmented AGC [3]. The 2DOF-PID adds a feedforward path from the measured local load disturbance:

$$\Delta P_{c,k}(s) = -\left[k_{p,k} + \frac{k_{i,k}}{s} + \frac{k_{d,k}\, s}{1+sT_f}\right] ACE_k(s) + K_{ff,L,k}\, \Delta P_{L,k}(s) \tag{12}$$

The 2DOF-PID-PV adds a second feedforward path from the measured PV active power of the area:

$$\Delta P_{c,k}(s) = -\left[k_{p,k} + \frac{k_{i,k}}{s} + \frac{k_{d,k}\, s}{1+sT_f}\right] ACE_k(s) + K_{ff,L,k}\, \Delta P_{L,k}(s) - K_{ff,PV,k}\, \Delta P_{PV,k}(s) \tag{13}$$

where $K_{ff,L,k}$ and $K_{ff,PV,k}$ are the load and PV feedforward gains. With the sign conventions of Section III-B, a load increase ($\Delta P_{L,k} > 0$) or a PV reduction ($\Delta P_{PV,k} < 0$) both raise the control signal. The PV path is practical because modern PV plant controllers report their real-time active power over SCADA, so $\Delta P_{PV,k}$ is available to the LFC controller. Ideally, the feedforward terms cancel a measured disturbance at its point of entry, so that the feedback part of the controller only has to correct the residual error. All three structures are tuned with the same Hybrid BBO-GWO optimiser and ITAE objective, so differences in performance can be attributed to the structure.

2.5 Disturbance Scenarios

Stage I uses SLPs of 0.1 p.u. and 0.5 p.u. applied to Area 1 only or to both areas, giving the four trials listed in Table II. Stage II combines a 0.1 p.u. SLP in both areas at $t = 1$ s with a PV cloud transient in Area 1 (Fig. 1): the PV output ramps down by 0.08 p.u. over 5 s, reaching its minimum at $t = 20$ s, and then ramps back to its pre-disturbance value over 6 s:

$$\Delta P_{PV,1}(t) = \begin{cases} 0, & t < 15 \\ -0.08\,\frac{t-15}{5}, & 15 \le t < 20 \\ -0.08\left(1 - \frac{t-20}{6}\right), & 20 \le t < 26 \\ 0, & t \ge 26 \end{cases} \tag{14}$$

The depth and ramp times were chosen to represent a severe but physically plausible cloud event: high-resolution measurements at large PV plants show that passing clouds can reduce plant output by a large fraction of its rating within seconds to tens of seconds [6]. The profile is thus a representative stress test rather than a reproduction of a specific measured record. Performance for the load step is evaluated over $t = 0$–12 s and for the PV transient over $t = 14$–34 s.

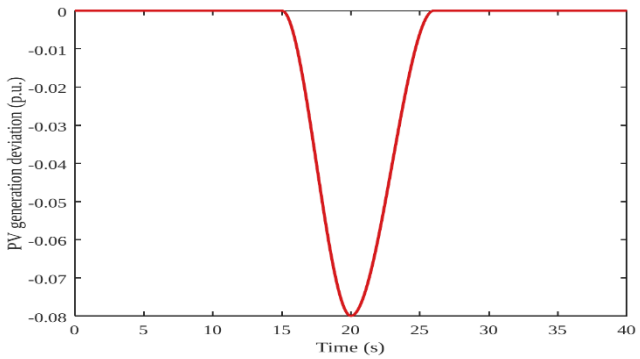


Fig. 1. Simulated PV generation deviation used as a time-varying disturbance: a 5 s ramp-down and 6 s ramp-up cloud transient of 0.08 p.u. superimposed on a 0.1 p.u. step load disturbance (MATLAB/ode45 output)

2.6 Objective Functions

The ISE, IAE and ITAE of an error signal $e(t)$ over a simulation horizon T are given, respectively, by:

$$ISE = \int_0^T [e(t)]^2 \, dt \tag{15}$$

$$IAE = \int_0^T |e(t)| \, dt \tag{16}$$

$$ITAE = \int_0^T t \, |e(t)| dt \tag{17}$$

ITAE was selected as the primary objective because its time weighting penalises errors that persist late in the response. The joint ITAE of the two frequency deviations and the tie-line power deviation for a disturbance scenario is:

$$J = \int_0^T t \left(|\Delta f_1| + |\Delta f_2| + \left|\Delta P_{tie,12}\right| \right) dt \tag{18}$$

In Stage I, the fitness minimised by each optimiser is the sum of J for a 0.1 p.u. SLP in Area 1 and a 0.1 p.u. SLP in Area 2, each over $T = 20$ s:

$$J_I = J|_{\Delta P_{L,1}=0.1} + J|_{\Delta P_{L,2}=0.1} \tag{19}$$

Using both single-area scenarios forces both area controllers to be effective; a fitness based on a disturbance in one area only allows the optimiser to weaken the controller of the other area without penalty. In Stage II, J is evaluated over the 34 s combined disturbance window. The per-area indices reported in the tables are computed from Δf_1 alone. Because the error indices combine frequency deviations in Hz and tie-line deviations in p.u., they are reported as unitless figures of merit.

2.7 Dynamic Performance Indices

The transient response of Area 1 is characterised by three time-domain indices, all expressed in physical units: the maximum frequency deviation $\max|\Delta f_1|$ (Hz), which defines the frequency nadir; the overshoot above the nominal frequency after the nadir (Hz); and the 2% settling time (s), defined as the time after which $|\Delta f_k(t) - \Delta f_k(T)|$ remains within 2% of the largest excursion of Δf_k from its final value.

2.8 Optimisation Algorithms

Each algorithm searches the six PID gains $\mathrm{x} = [k_{p1}, k_{i1}, k_{d1}, k_{p2}, k_{i2}, k_{d2}]$ within $k_p \in [0,5]$, $k_i \in [0,5]$ and $k_d \in [0,1]$. In Stage I, every algorithm uses a population of 30, 100 iterations and J_I (Eq. (19)) as the fitness. In Stage II, the decision vector is extended with the feedforward gains of the structure being tuned, and a population of 16 with 30 iterations is used.

2.8.1 Brown bear optimisation (BBO): BBO [11] is a population-based metaheuristic in which each bear represents a candidate solution. As shown in Fig. 2, in each iteration a bear is relocated at random within the search bounds with probability 0.1 (migration); otherwise, it makes, with equal probability, an exploration moves towards a randomly selected bear or an exploitation move towards the best bear found so far:

$$X_i^{t+1} = X_i^t + r_1 (X_{rand} - X_i^t) \tag{20}$$

$$X_i^{t+1} = X_i^t + r_2 (X_{best} - X_i^t) \tag{21}$$

$$X_i^{t+1} = LB + r_3(UB - LB) \quad (22)$$

where X_i^t is the position of bear i at iteration t, X_{rand} is a randomly selected bear, X_{best} is the best bear, LB and UB are the lower and upper bounds of the decision variables, and r_1, r_2 and r_3 are uniform random vectors in $[0,1]$. A new position replaces the old one only if its fitness is better (greedy selection).

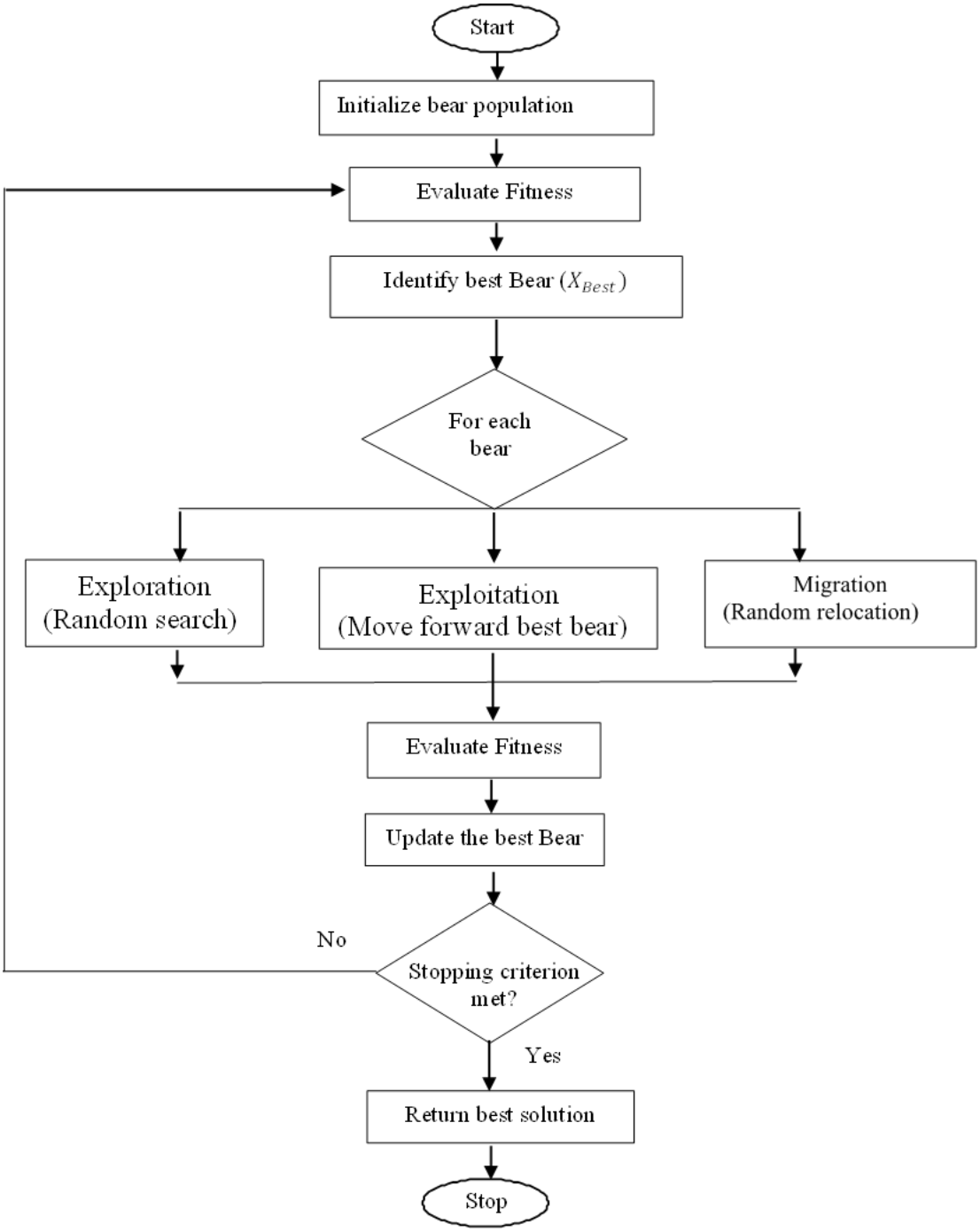


Fig. 2. Flowchart of Brown Bear Optimisation (BBO)

2.8.2 Political optimiser (POA): POA [12] divides the population into political parties and constituencies; here the 30 members form 6 parties of 5 members. Each member updates its position with respect to its party leader and the winner of its constituency using the recent-past-based position-updating strategy, and the algorithm alternates election campaign, party switching (with a switching rate decreasing linearly from 1 to 0), inter-party election and parliamentary affairs phases, which gives it a strong cooperative exploitation ability.

2.8.3 Grey wolf optimisation (GWO): GWO [13] is a population-based metaheuristic inspired by the social hierarchy and hunting behaviour of grey wolves. Each wolf represents a candidate solution. The alpha wolf

(α) is the best solution, the beta wolf (β) the second best, the delta wolf (δ) the third best, and the omega wolves (ω) the remaining solutions. Hunting consists of encircling, hunting and attacking the prey, led by the α, β and δ wolves (Fig. 3). The position update is:

$$A = 2ar_1 - a, \qquad C = 2r_2, \qquad a = 2 - \frac{2t}{T_{max}} \tag{23}$$

$$D_\alpha = |C_1 X_\alpha - X|, \quad D_\beta = |C_2 X_\beta - X|, \quad D_\delta = |C_3 X_\delta - X| \tag{24}$$

$$X_1 = X_\alpha - A_1 D_\alpha, \quad X_2 = X_\beta - A_2 D_\beta, \quad X_3 = X_\delta - A_3 D_\delta \tag{25}$$

$$X(t+1) = \frac{X_1 + X_2 + X_3}{3} \tag{26}$$

where t is the current iteration, T_{max} is the maximum number of iterations, a decreases linearly from 2 to 0, r_1 and r_2 are uniform random vectors in $[0,1]$, X_α, X_β and X_δ are the positions of the three best wolves, and X is the position of the current wolf.

2.8.4 Hybrid BBO-GWO: The Hybrid BBO-GWO algorithm (Fig. 4) uses BBO for exploration and GWO for exploitation. After initialisation, the population is evaluated and the three best solutions (α, β, δ) and the best bear are identified. In each iteration, every solution i draws a uniform random number $r_s \in [0,1]$ and a candidate position is generated by:

$$X_i^{new} = \begin{cases} X_i^t + r(X_{rand} - X_i^t), & r_s < P \text{ (BBO phase)} \\ \frac{X_1 + X_2 + X_3}{3}, & r_s \geq P \text{ (GWO phase)} \end{cases} \tag{27}$$

where P is the switching probability, set to $P = 0.5$, r is a uniform random vector in $[0,1]$, and X_1, X_2 and X_3 are computed from Eq. (25) using the current α, β and δ. The candidate is clipped to the search bounds and accepted only if it improves the fitness of solution i:

$$X_i^{t+1} = \begin{cases} \min(\max(X_i^{new}, LB), UB), & \text{if it improves } J_I \\ X_i^t, & \text{otherwise} \end{cases} \tag{28}$$

after which α, β, δ and the best bear are updated. The loop stops when the maximum number of iterations is reached and returns α as the optimal gain vector. Taking the expectation over r_s, the candidate generation is on average a weighted combination of the two moves:

$$E[X_i^{new}] = w_1 X_{BBO} + w_2 X_{GWO}, \qquad w_1 = P, \quad w_2 = 1 - \qquad P, \quad w_1 + w_2 = 1 \tag{29}$$

The motivation for the hybrid is complementary search behaviour. The BBO move towards a randomly selected bear keeps the population diverse, while the GWO move, which averages three leader-guided positions with a step size that shrinks as a decreases, refines the solution around the best region found. As an ablation, a variant with an adaptive switching probability decreasing linearly from 0.9 to 0.1 (more exploration early, more exploitation late) was also evaluated.

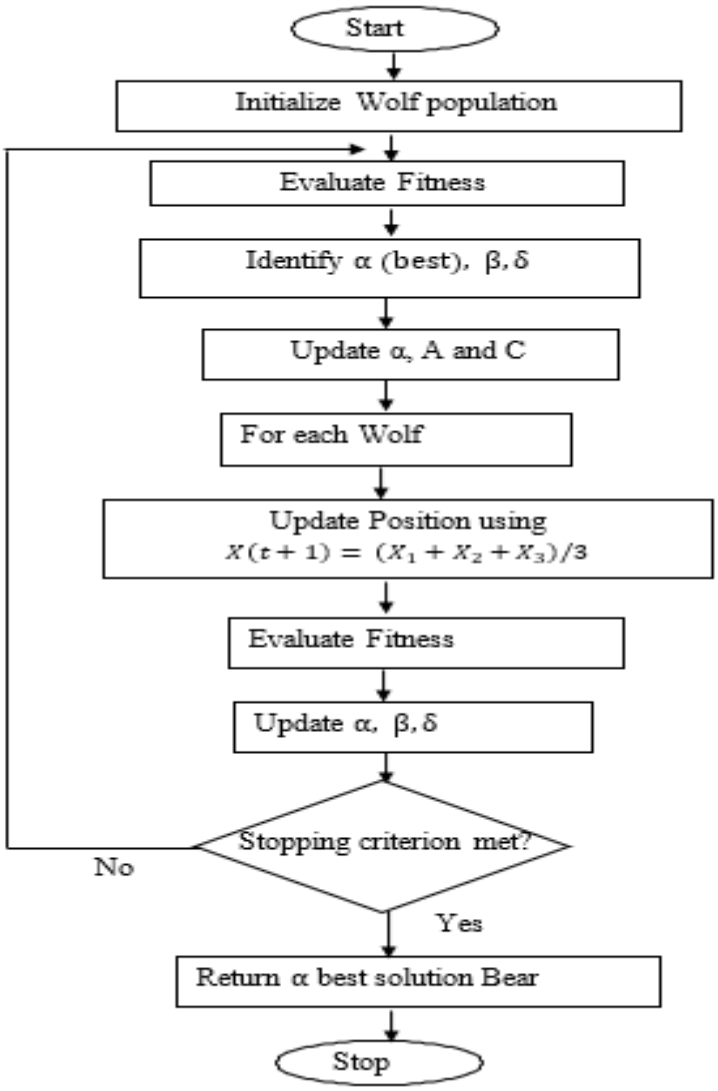


Fig. 3: Grey Wolf Algorithm Flow Chart

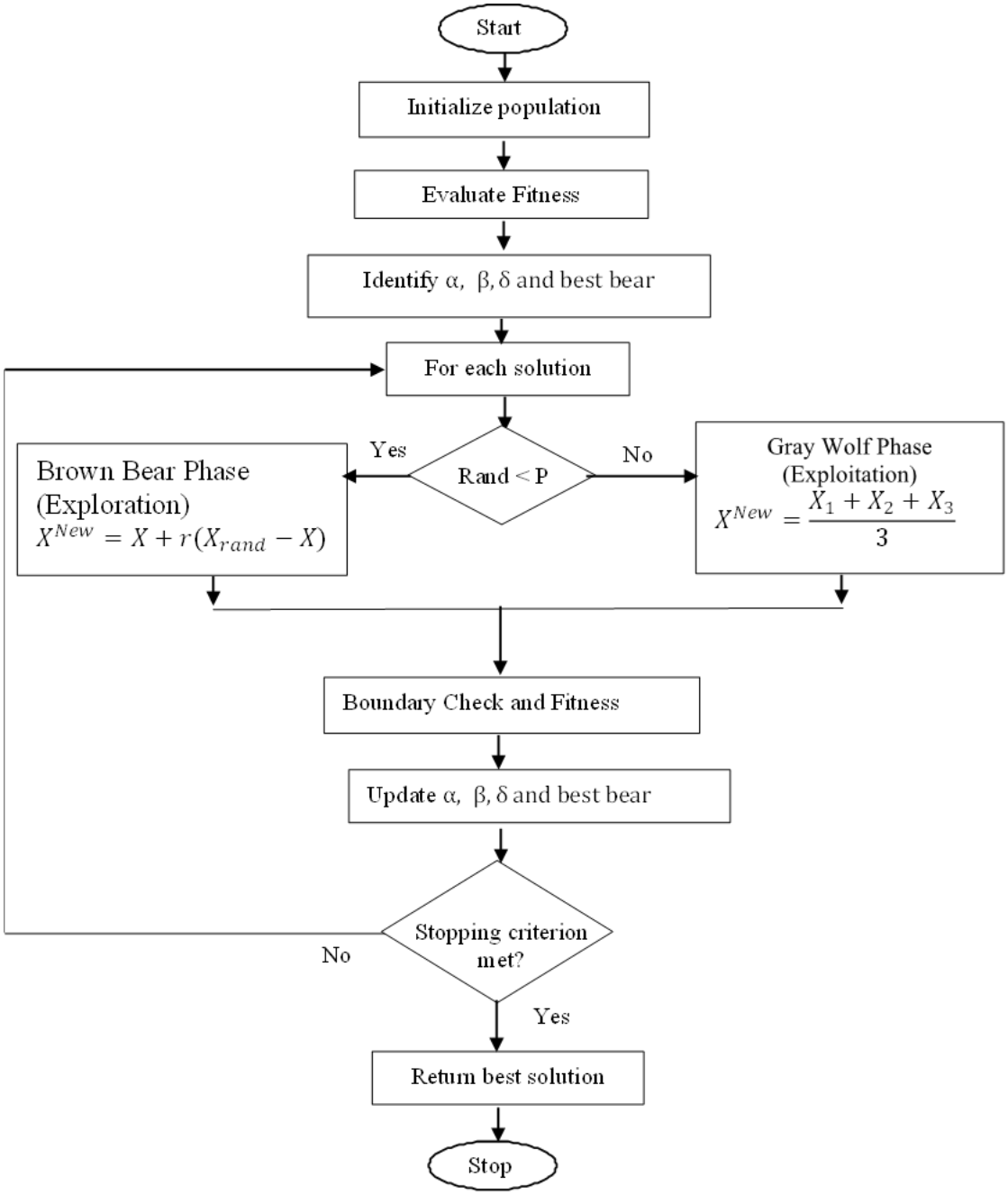


Fig. 4. Flowchart of the hybrid Brown Bear–Grey Wolf Optimisation (Hybrid BBO-GWO) algorithm

2.8.5 Benchmark Algorithms: *PSO and GA:* To assess the hybrid against established optimisers, PSO [21] and a real-coded GA [20] were also applied with the same population, iteration budget and bounds. PSO uses an inertia weight decreasing linearly from 0.9 to 0.4, acceleration coefficients $c_1 = c_2 = 2$ and a velocity limit of 20% of the search range. The GA uses binary tournament selection, blend (BLX-0.5) crossover with probability 0.9, Gaussian mutation with probability 0.1 per gene and a standard deviation of 10% of the search range, and an elite of two individuals.

2.9 Statistical and Robustness Evaluation

Because metaheuristics are stochastic, each of the six Stage I algorithms, together with the adaptive-P hybrid ablation, was run 30 times independently. In run r, all algorithms start from the same random initial population, so that differences between algorithms are not caused by initialisation. For each algorithm, the best, worst, mean and median final fitness, its standard deviation, the mean convergence curve, and the number of successful runs are reported; a run is counted as successful when its final fitness is within 1% of the best value found by any algorithm. The significance of the difference between Hybrid BBO-GWO and each other algorithm is assessed with the two-sided Wilcoxon rank-sum test at the 5% level, and the mean rank of each algorithm over all runs is also given.

The robustness of the optimised controller was tested by applying the best gains found by each algorithm, without retuning, to perturbed plants. The inertia constant H, load-damping coefficient D, governor and turbine time constants T_g and T_t, speed regulation R, tie-line coefficient T_{12} and the SLP magnitude were each changed by −20%, −10%, +10% and +20%, one at a time, with the frequency-bias factor of the controller kept at its nominal value. An increasing PV share in Area 1 was represented by reducing the synchronous inertia of Area 1 by 10%, 20% and 30%. For each case, stability, J_I and the Area 1 frequency nadir and settling time were recorded.

2.10 Simulation Procedure

Stage I was carried out in four steps: (i) the system without secondary control was subjected to the four SLP trials (0.1 p.u. and 0.5 p.u. in Area 1 only or in both areas); (ii) a PID controller tuned by trial and error ($k_p = k_i = 0.5$ and $k_d = 0.1$ in both areas) was added and the same SLPs were applied; (iii) the PID gains were optimised with BBO, POA, GWO, PSO, GA and Hybrid BBO-GWO over 30 runs each, and the SLPs were reapplied with the best gains; and (iv) the robustness tests of Section III-I were performed. In Stage II, the feedback-only PID, 2DOF-PID and 2DOF-PID-PV were tuned with Hybrid BBO-GWO on the combined disturbance of Section III-E by minimising J over the 34 s disturbance window, and each tuned controller was then evaluated separately on the load-step and PV-transient windows. The MATLAB code used for both stages is available from the corresponding author on reasonable request.

3. RESULTS AND DISCUSSION

3.1 Stage I: Tuning Comparison for the Feedback PID

All Stage I results in this section are direct outputs of the MATLAB state-space implementation described in Section III-A.

3.1.1 System without secondary control: Without secondary control, the system relies on primary governor droop, which limits but cannot remove the frequency deviation. Table 2 summarises the error indices, the steady-state frequency and the maximum frequency deviation for the four SLP trials.

Table 2: Error Indices and Frequency Performance of the System without Secondary Control (T = 20 S)

Trial	Step load perturbation	Joint ISE	Joint IAE	Joint ITAE	Steady-state frequency (Hz)	Max. deviation, Area 1 (Hz)
1	0.1 p.u. both areas	4.463	9.403	94.17	49.76	0.307
2	0.1 p.u. Area 1 only	1.631	5.682	57.08	49.88	0.224
3	0.5 p.u. Area 1 only	40.770	28.409	285.40	49.41	1.118
4	0.5 p.u. both areas	111.565	47.013	470.87	48.82	1.535

In every trial, the frequency settles below 50 Hz: at 49.76 Hz and 49.88 Hz for 0.1 p.u. SLPs in both areas and in Area 1 only, and at 48.82 Hz and 49.41 Hz for the corresponding 0.5 p.u. SLPs. These offsets agree with the steady-state value $\Delta f = -\Delta P_L/(B_1 + B_2)$ expected from primary control alone, and the two areas settle to the same frequency. A sustained offset of this size would lead to under-frequency load shedding in a real system (Fig. 5).

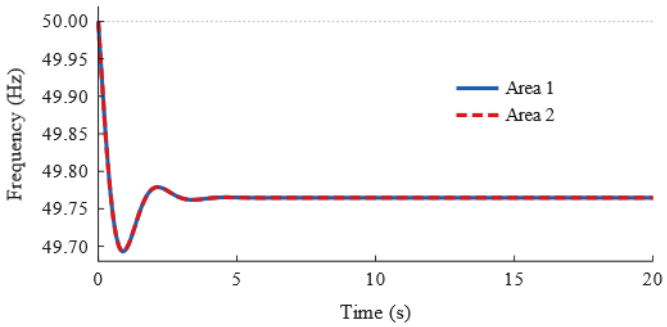


Fig. 5. Frequency response of Areas 1 and 2 without secondary control for a 0.1 p.u. SLP in both areas (the two curves coincide). The frequency settles at 49.76 Hz

3.1.2 Conventional PID Control: A PID secondary loop with gains chosen by trial and error ($k_p = k_i = 0.5, k_d = 0.1$ in both areas) removes the steady-state error, as shown in Table 3 and Fig. 6.

TABLE 3: Performance of the system without secondary control and with the trial-and-error PID

Metric	Without secondary control	Trial-and-error PID	Change
Final frequency, Area 1, 0.1 p.u. SLP in both areas (Hz)	49.76	50.00	Restored
Joint ITAE, 0.1 p.u. SLP in both areas	94.17	2.455	97.4% reduction
Joint ITAE, 0.5 p.u. SLP in both areas	470.87	12.273	97.4% reduction
Max. frequency deviation, Area 1, 0.1 p.u. SLP in both areas (Hz)	0.307	0.212	31.0% smaller
Settling time, Area 1, 0.5 p.u. SLP in both areas (s)	2.70*	9.80	–

Settles quickly, but to 48.82 Hz rather than 50 Hz

With PID control, the offset is eliminated and 50.00 Hz is restored in all trials, with the joint ITAE reduced by 97.4% relative to the system without secondary control for both the 0.1 p.u. and 0.5 p.u. SLPs in both areas. The response is well damped, without overshoot above 50 Hz, but slow: the settling time of Area 1 is 8.3–9.8 s. A fixed-gain PID acting on the ACE therefore removes the steady-state error, and the remaining question is how much systematic tuning of the gains improves the transient performance.

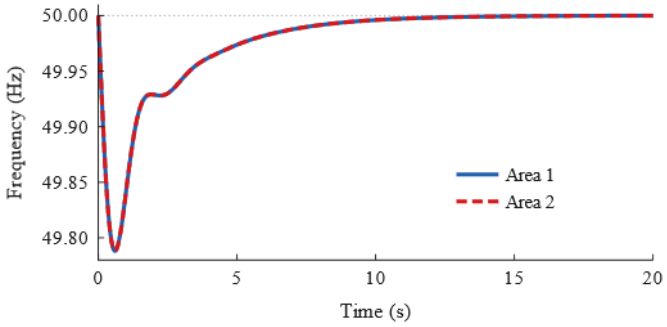


Fig. 6. Frequency response with the trial-and-error PID for a 0.1 p.u. SLP in both areas (the two curves coincide). The nominal frequency is recovered within approximately 10 s

3.1.3 Metaheuristic tuning and statistical comparison: Table 4 lists the best gains found by each algorithm over 30 runs, the corresponding fitness J_I, and the Area 1 ITAE for a 0.1 p.u. SLP in Area 1 together with its reduction relative to the trial-and-error PID (0.5222).

Table 4: Best PID gains over 30 runs, fitness and Area 1 ITAE (0.1 p.u. SLP in Area 1)

Algorithm	k_{p1}	k_{i1}	k_{d1}	k_{p2}	k_{i2}	k_{d2}	J_I	Area 1 ITAE	Reduction (%)
BBO	2.016	4.732	0.615	2.752	4.584	0.906	0.11395	0.02700	94.8
POA	3.056	5.000	1.000	2.141	5.000	0.655	0.10510	0.02216	95.8
GWO	2.142	5.000	0.655	3.050	5.000	1.000	0.10510	0.02524	95.2
PSO	2.141	5.000	0.655	3.056	5.000	1.000	0.10510	0.02524	95.2
GA	2.141	5.000	0.655	3.056	5.000	1.000	0.10510	0.02524	95.2
Hybrid BBO-GWO	2.141	5.000	0.656	3.053	5.000	1.000	0.10510	0.02523	95.2

All six algorithms reduce the Area 1 ITAE of the trial-and-error PID by about 95%. Five of them (POA, GWO, PSO, GA and Hybrid BBO-GWO) converge to the same optimum ($J_I = 0.10510$), at which the integral gains reach their upper bound ($k_i = 5$) and one derivative gain reaches its bound ($k_d = 1$). Two mirror-image gain sets attain this optimum, with the larger proportional gain in either Area 1 or Area 2, which explains why the Area 1 ITAE differs slightly between algorithms with the same J_I. Standalone BBO stops at a clearly worse solution ($J_I = 0.11395$).

Table 5 summarises the 30-run statistics. Hybrid BBO-GWO reached the best-known fitness (within 1%) in all 30 runs, whereas standalone BBO never did, and its mean fitness is 19.4% lower than that of BBO ($p < 0.001$). This confirms that the GWO phase removes the premature stagnation of BBO. The hybrid is statistically equivalent to standalone GWO ($p = 0.22$). PSO and GA reach the optimum marginally more consistently: their mean fitness and spread are lower than those of the hybrid and the difference is statistically significant, but the difference in mean fitness between PSO and the hybrid is only 0.013%, which has no practical effect on the closed-loop response. POA, like PSO and GA, has a median at the optimum and a better mean rank than the hybrid, but one run stopped at 0.1085 (29 of 30 successful runs), giving it the largest spread among the five competitive algorithms. The adaptive-P variant behaves like the fixed-P hybrid ($p = 0.42$), so the result is not sensitive to the switching rule.

Table 5: Statistics of the final fitness J_I over 30 independent runs (population 30, 100 iterations)

Algorithm	Best	Worst	Mean	Median	Std	Successful runs	Mean rank	Wilcoxon p (vs. hybrid)
BBO	0.11395	0.14307	0.13036	0.13072	7.9e-03	0/30	195.5	< 0.001
POA	0.10510	0.10848	0.10523	0.10510	6.2e-04	29/30	54.0	< 0.001
GWO	0.10510	0.10546	0.10512	0.10510	6.7e-05	30/30	126.5	0.22
PSO	0.10510	0.10510	0.10510	0.10510	4.0e-07	30/30	34.3	< 0.001
GA	0.10510	0.10510	0.10510	0.10510	6.8e-07	30/30	62.9	< 0.001
Hybrid BBO-GWO	0.10510	0.10530	0.10511	0.10511	3.6e-05	30/30	135.7	–
Hybrid BBO-GWO, adaptive P	0.10510	0.10511	0.10511	0.10510	3.7e-06	30/30	129.5	0.42

Figure 7 shows the mean convergence over the 30 runs. PSO and POA come within 1% of the optimum by iteration 11, GA by iteration 27, the hybrid by iteration 34 and GWO by iteration 43, while BBO stagnates near $J_I \approx 0.13$. Figure 8 shows the distribution of the final fitness: all algorithms except BBO are tightly concentrated at the optimum. These results show that, for this problem, the choice among competent metaheuristics has a negligible effect on the tuned controller, whereas the choice between systematic tuning and trial and error has a large one.

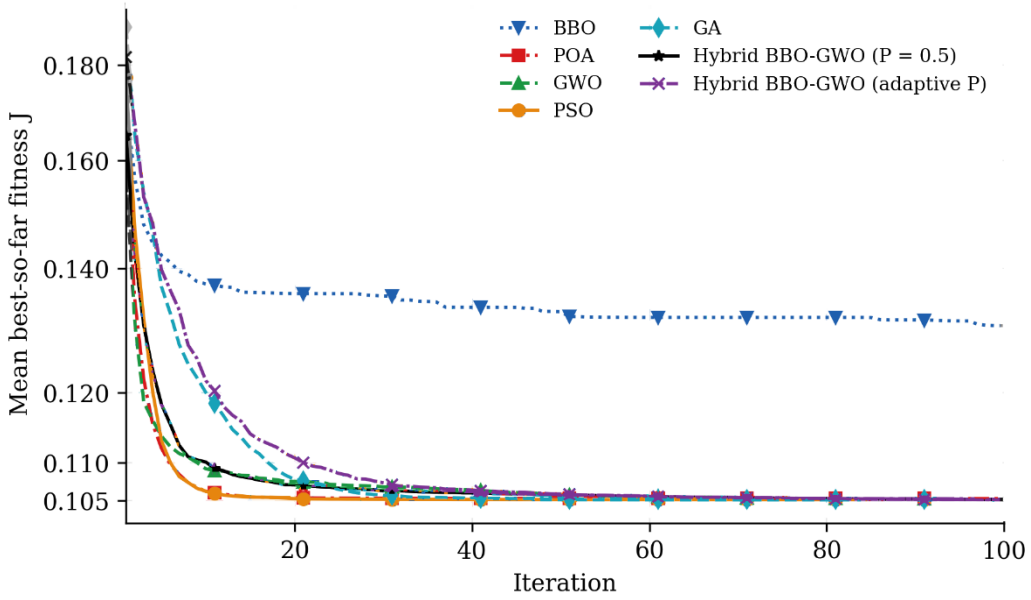


Fig. 7. Mean best-so-far fitness over 30 independent runs for each algorithm (population 30)

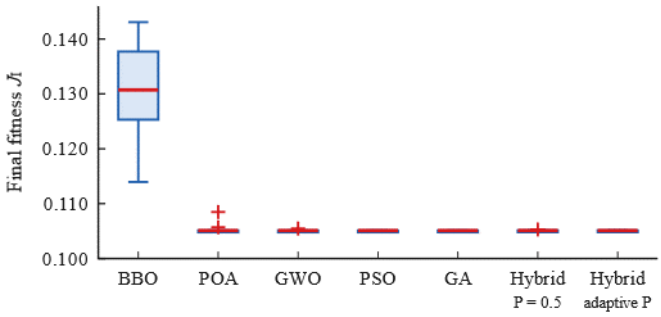


Fig. 8. Distribution of the final fitness over 30 independent runs

3.1.4 Hybrid BBO-GWO-Tuned PID Versus Trial-and-Error PID: Table 6 compares the Hybrid BBO-GWO-tuned PID with the trial-and-error PID for a 0.1 p.u. SLP in Area 1.

Table 6: Performance of the Hybrid BBO-GWO-tuned PID versus the trial-and-error PID (0.1 p.u. SLP in Area 1)

Metric	Trial-and-error PID	Hybrid BBO-GWO PID	Change
ITAE, Area 1	0.5222	0.02523	95.2% reduction
ISE, Area 1	0.01846	0.002797	84.8% reduction
IAE, Area 1	0.2352	0.04748	79.8% reduction
Max. frequency deviation, Area 1 (Hz)	0.1711	0.0982	42.6% smaller
Overshoot above 50 Hz, Area 1 (Hz)	0.0000	0.0243	Small overshoot introduced
Settling time, Area 1 (s)	8.26	2.34	71.7% reduction
Settling time, Area 2 (s)	10.33	2.63	74.5% reduction
Final frequency (Hz)	50.00	50.00	Maintained

The tuned controller reduces the Area 1 ITAE by 95.2%, the ISE by 84.8% and the IAE by 79.8%, makes the frequency dip 42.6% shallower and shortens the settling time from 8.26 s to 2.34 s in Area 1 and from 10.33 s to 2.63 s in Area 2. The price is a small overshoot of 0.024 Hz above 50 Hz, compared with none for the slower trial-and-error controller. Figure 9 shows the response of the tuned controller to a severe 0.5 p.u. SLP in both areas, and Fig. 10 compares the three cases for the same disturbance: the system without secondary control settles quickly but at 48.82 Hz, the trial-and-error PID recovers 50 Hz slowly, and the Hybrid BBO-GWO-tuned PID recovers it within about 2 s with a much shallower dip. Over the four trials, the tuned PID reduces the joint ITAE of the trial-and-error PID by 96.6–97.6%.

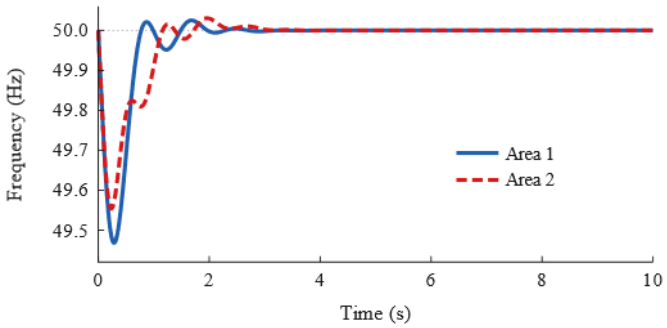


Fig. 9. Frequency response with the Hybrid BBO-GWO-tuned PID for a severe 0.5 p.u. SLP in both areas

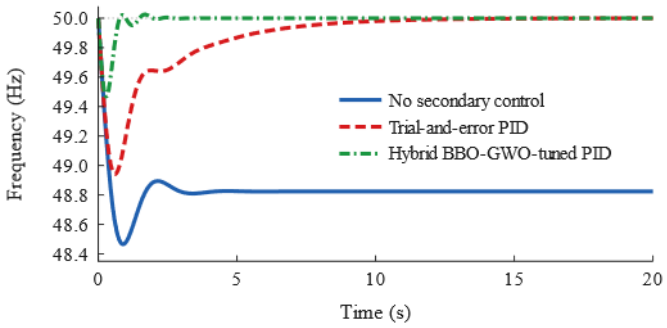


Fig. 10. Area 1 frequency without secondary control, with the trial-and-error PID and with the Hybrid BBO-GWO-tuned PID for a severe 0.5 p.u. SLP in both areas

3.1.5 Robustness to Parameter Variations: Table 7 lists the change in the fitness J_I of the Hybrid BBO-GWO-tuned PID when each plant parameter is varied without retuning. The closed loop remained stable in all 31 cases, for the best gains of every algorithm. For the hybrid gains, the Area 1 frequency never fell below 49.88 Hz for the 0.1 p.u. SLP, and the settling time never exceeded 3.1 s.

Table 7: Change in fitness J_I (%) of the Hybrid BBO-GWO-tuned PID under parameter variations (no retuning)

Parameter varied	−20%	−10%	+10%	+20%
Inertia constant H	+9.7	+2.6	-0.4	+1.4
Load damping D	+0.2	+0.1	-0.1	-0.2
Governor time constant T_g	-8.0	-5.5	+11.1	+31.6
Turbine time constant T_t	-7.1	-4.8	+9.4	+27.1
Speed regulation R	+3.5	+1.3	-0.7	-0.8
Tie-line coefficient T_{12}	+3.1	+0.0	+3.7	+12.7
SLP magnitude	-20.0	-10.0	+10.0	+20.0
PV share in Area 1 (10%, 20%, 30%)	–	+5.8	+19.5	+41.2

The controller is insensitive to D (below 0.3%) and only mildly sensitive to H, R and T_{12} (within about 13%). The largest effects come from slower governor and turbine dynamics (+31.6% and +27.1% for +20% in T_g and T_t) and from a higher PV share, which reduces inertia (+41.2% at 30%); changes in the SLP magnitude scale J_I proportionally, as expected for a linear system (Fig. 11). Figure 12 shows that even in the worst cases the response remains well damped and returns to 50 Hz within about 3 s. The best gains of the other algorithms behave similarly, with worst-case increases of 31.5–41.4%, caused by either the 30% PV share or a 20% slower governor.

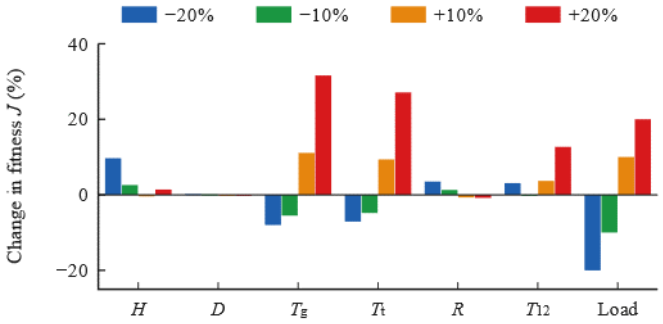


Fig. 11. Change in the fitness of the Hybrid BBO-GWO-tuned PID for ±10% and ±20% parameter variations

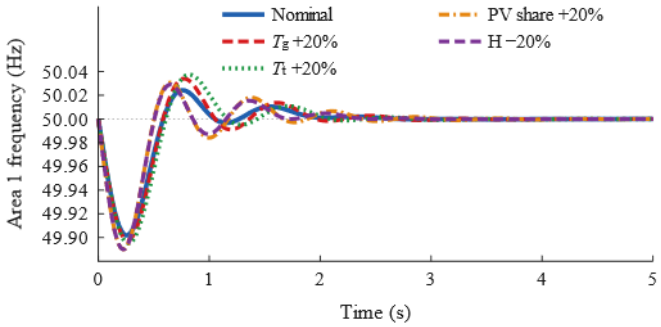


Fig. 12. Area 1 frequency of the Hybrid BBO-GWO-tuned PID for the nominal plant and the most influential parameter variations (0.1 p.u. SLP in Area 1)

3.1.6 Discussion of Stage I: Secondary control is essential in this system, whatever the tuning method, which agrees with the literature on low-inertia systems [4], [17]. Systematic tuning brings large gains over trial and error: every metaheuristic reduced the Area 1 ITAE of the trial-and-error PID by about 95%. The comparison between metaheuristics is more nuanced. Hybrid BBO-GWO clearly improves on standalone BBO, reaching the optimum in 30 of 30 runs instead of 0 of 30, and matches GWO, but it does not outperform PSO, GA or POA on this problem, in which the optimum lies on the boundary of the search space and is found by all competent algorithms. This is consistent with the no-free-lunch theorem [10] and indicates that, for PID-based LFC of this benchmark, the choice of metaheuristic is a secondary design decision.

3.2 Stage II: Controller Structure Comparison

Although well-tuned, a feedback-only PID can act only after the frequency has deviated. Stage II evaluates whether adding feedforward paths, and in particular a path from measured PV power, improves performance when PV variability is present. All Stage II figures are direct MATLAB (ode45) outputs of the two-area ODE model, with the gains optimised by the Hybrid BBO-GWO procedure of Section III-H4.

3.2.1 Optimisation and convergence: Table 8 lists the gains obtained by minimising J over the 34 s disturbance window for each structure, with a population of 16 and 30 iterations. Several gains reached the upper bounds of the search space ($k_{p1} = 5.0$, $k_i = 5.0$ and $k_d = 1.0$ for the PID and 2DOF-PID), which indicates that wider bounds could improve these two structures and should be examined in future work. To check that the conclusions do not depend on the solver, the complete model and optimisation procedure were implemented independently in MATLAB (ode45) and Python (SciPy solve_ivp); the optimised gains agreed, apart from minor differences caused by the stochastic search.

Table 8: Hybrid BBO-GWO-optimised gains for the feedback-only PID, 2DOF-PID and 2DOF-PID-PV controllers for the combined load-step and PV-transient disturbance (MATLAB run); the resulting joint ITAE over the 34 s window is 1.676, 1.597 and 0.412, respectively

Controller	k_{p1}	k_{i1}	k_{d1}	k_{ff}, **L1**	k_{ff}, **PV1**	k_{p2}	k_{i2}	k_{d2}	k_{ff}, **L2**	k_{ff}, **PV2**
PID	5.000	5.000	0.963	-	-	4.709	5.000	0.987	-	-
2DOF-PID	5.000	5.000	1.000	0.510	-	4.921	4.470	1.000	0.609	-
2DOF-PID-PV	4.120	5.000	1.000	0.756	0.950	2.349	1.355	0.982	0.807	1.139

Figure 13 shows the convergence of the three optimisations. The 2DOF-PID-PV run has a markedly lower ITAE throughout most of the iterations and converges to a lower value than the other two structures within the first 10–15 iterations.

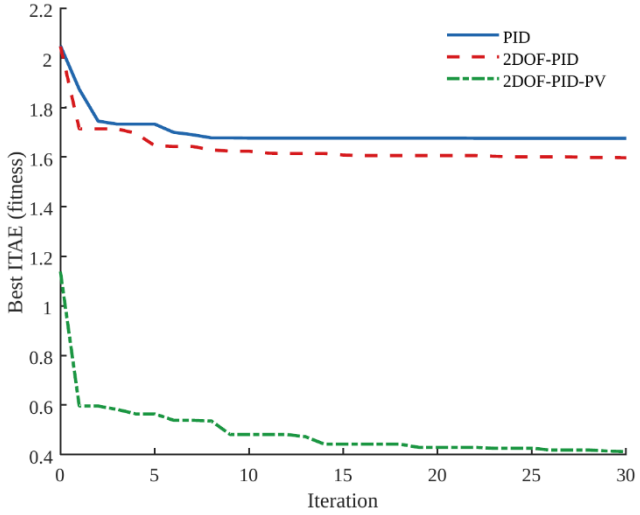


Fig. 13. Hybrid BBO-GWO convergence (best-so-far joint ITAE) for the feedback-only PID, 2DOF-PID and 2DOF-PID-PV controllers on the combined load-step and PV-transient disturbance (MATLAB/ode45 output)

3.2.2 Load-Step Disturbance Rejection: Table 9 compares the three controllers for the 0.1 p.u. SLP, evaluated over $t = 0$–12 s. Percentage changes relative to the PID are shown in parentheses.

Table 9: Load-step disturbance rejection performance, Area 1 (MATLAB run)

Metric (Area 1)	PID	2DOF-PID	2DOF-PID-PV
ITAE	0.0857	0.0462 (-46.1%)	0.0493 (-42.5%)
ISE	0.00197	0.00128 (-35.0%)	0.00122 (-38.1%)
Frequency nadir (Hz)	49.9158	49.9245 (10.3% shallower)	49.9263 (12.5% shallower)
Settling time (s)	4.05	3.23 (−20.2%)	3.35 (−17.3%)

Both 2DOF structures clearly outperform the feedback-only PID on the load step. The 2DOF-PID reduces the ITAE by 46.1% and the ISE by 35.0%, the frequency nadir is 10–13% shallower, and the settling time is 17–20% shorter. As expected, the 2DOF-PID and 2DOF-PID-PV perform similarly here, because this window contains no PV transient (Fig. 14).

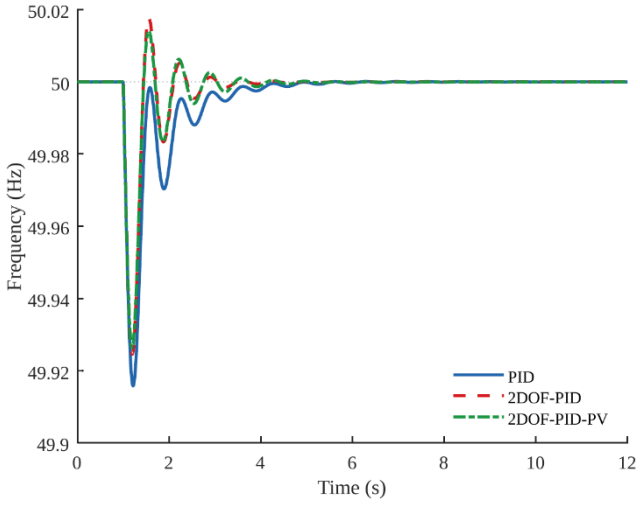


Fig. 14. Frequency response of Area 1 to the 0.1 p.u. SLP with the feedback-only PID, 2DOF-PID and 2DOF-PID-PV (MATLAB/ode45 output)

3.2.3 PV cloud-transient rejection: Table 10 compares the three controllers for the PV cloud transient of Section III-E, evaluated over $t = 14$–34 s.

Table 10: PV cloud-transient rejection performance, Area 1 (MATLAB run)

Metric (Area 1)	PID	2DOF-PID	2DOF-PID-PV
ITAE	0.2442	0.2445 (+0.1%)	0.0518 (-78.8%)
IAE	0.0366	0.0367 (+0.1%)	0.0081 (-78.0%)
Extreme frequency (Hz)	49.9946	49.9946	50.0013

This is the key result of Stage II. The feedforward path of the 2DOF-PID measures only the local load disturbance and therefore gives no benefit against the PV transient: the feedback-only PID and 2DOF-PID responses practically coincide (Fig. 15), and the ITAE and IAE of the 2DOF-PID are even marginally (0.1%) higher. A controller can only compensate directly for a disturbance that it measures. The 2DOF-PID-PV, which uses PV power telemetry, largely cancels the PV transient, reducing the ITAE by 78.8% and the IAE by 78.0%. Its extreme frequency moves from slightly below 50 Hz to slightly above it (50.0013 Hz), which indicates that the ITAE-optimal PV feedforward gain in Eq. (13) slightly overcompensates the disturbance. The MATLAB and Python implementations reproduced the reduction of approximately 79% in ITAE and IAE within about 1% of each other across repeated optimisations, which supports the view that this is a property of the control structure rather than of a particular solver.

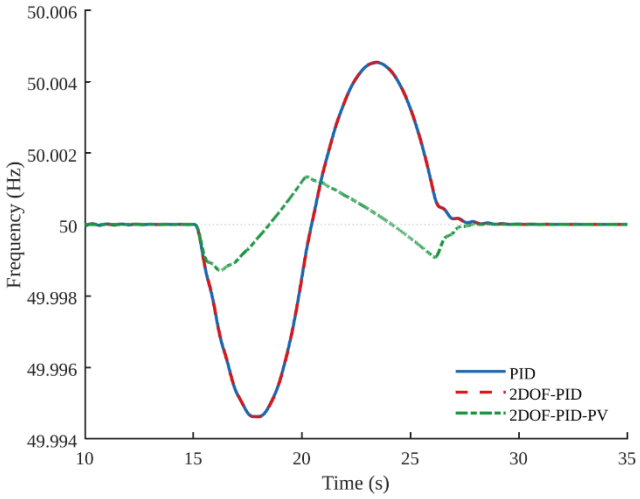


Fig. 15. Frequency response of Area 1 to the PV cloud transient. The feedback-only PID and 2DOF-PID responses coincide, while the 2DOF-PID-PV reduces the ITAE by 78.8% (MATLAB/ode45 output)

Figure 16 shows the complete 40 s response of Area 1 for the three controllers, combining the load step at $t = 1$ s and the PV cloud transient between $t = 15$ s and $t = 26$ s.

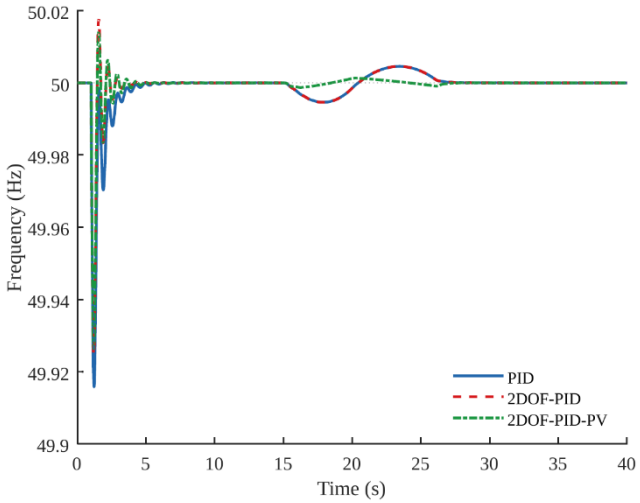


Fig. 16. Full 40 s simulated frequency response of Area 1 for the three controllers, combining the SLP at t = 1 s and the PV cloud transient between t = 15 s and 26 s (MATLAB/ode45 output)

3.2.4 Discussion of Stage II: Load feedforward is a low-cost enhancement to a well-tuned PID: the 2DOF-PID nearly halves the ITAE of the load step without compromising performance on the PV transient. It does not, however, improve the response to the PV transient, because it cannot observe it. The 2DOF-PID-PV, which observes the PV disturbance directly through telemetry, reduces both the ITAE and the IAE of the PV transient by about 78–79%, while performing similarly to the 2DOF-PID on the load step. The contrast with Stage I is instructive: there, replacing one competent metaheuristic with another changed the mean fitness by less than 0.2%, whereas here, with the optimiser fixed, adding the PV feedforward path reduced the PV-transient ITAE by 78.8%. The benefit of feedforward depends on the accuracy of the measured signal; errors or delays in the PV telemetry would reduce it, and this should be quantified in future work. Where PV telemetry is available, the 2DOF-PID-PV is therefore the preferred structure in terms of disturbance rejection, at the cost of requiring PV power telemetry, and renewable-aware feedforward paths merit further study in two-area and multi-area LFC.

3.3 Limitations

The following limitations should be considered when interpreting the results. First, the study uses a single two-area linear benchmark rather than a validated model of the Nigerian grid (Section III-C), and governor dead-band, generation rate constraints and communication delays are not modelled. Second, in Stage I the optimum lies on the upper bounds of the integral and derivative gains, so the ranking of the algorithms may change with wider bounds or a more demanding, non-linear plant. Third, the Stage II gains were obtained with a smaller budget (population 16, 30 iterations), and only the 2DOF-PID-PV result was confirmed across repeated optimisations; the robustness of the feedforward structures to errors and delays in the PV telemetry has not yet been quantified.

4. CONCLUSION

This paper evaluated LFC of a two-area benchmark power system with solar PV using a unified two-stage framework that separates the effect of controller tuning from that of controller structure. The following findings were demonstrated on the benchmark. Without secondary control, the frequency settles below 50 Hz after every tested disturbance, at 49.76 Hz for a 0.1 p.u. SLP in both areas and at 48.82 Hz for a 0.5 p.u. SLP in both areas. A trial-and-error PID restores 50 Hz and reduces the joint ITAE by 97.4%, but settles slowly (8.3–9.8 s). Metaheuristic tuning reduces the Area 1 ITAE of the trial-and-error PID by about 95% and shortens the settling time to about 2.3 s. Over 30 independent runs, Hybrid BBO-GWO reached the best-known fitness in every run and lowered the mean fitness of standalone BBO by 19.4%; it was statistically equivalent to GWO, while PSO and GA reached the same optimum marginally more consistently. The tuned controller remained stable under ±20% parameter variations and a 30% PV share. Changing the controller structure has a larger effect than changing the metaheuristic. Load feedforward (2DOF-PID) nearly halves the ITAE of the load step (−46.1%) but gives no benefit on the PV cloud transient (+0.1%), because it does not observe it. Adding a PV feedforward path from real-time PV telemetry (2DOF-PID-PV) reduces the PV-transient ITAE by 78.8% and the IAE by 78.0%. Systematic tuning is therefore worthwhile, but once a competent optimiser is used, further gains come from giving the controller a measurement of the disturbance rather than from a different metaheuristic. For the Nigerian grid, these results are indicative rather than predictive. They suggest that, as PV capacity grows, making PV plant active-power telemetry available to the secondary frequency controller could be more valuable than refining the tuning of existing PID loops. Confirming this requires a model built from Nigerian system data. Future work will extend the study to larger test systems (e.g., the IEEE 39-bus and 118-bus systems) and to a model of the Nigerian grid; include governor dead-band, generation rate constraints and communication delays; quantify the sensitivity of the PV feedforward to telemetry error and delay; widen the gain bounds and consider fractional-order controllers; and investigate forecast-aware PV compensation, coordination with fast storage (battery, SMES and flywheel) and hardware-in-the-loop validation.

REFERENCES

[1] O. I. Elgerd, *Electric Energy Systems Theory: An Introduction*. New York, NY, USA: McGraw-Hill, 1971.
[2] P. Kundur, *Power System Stability and Control*. New York, NY, USA: McGraw-Hill, 1994.
[3] H. Bevrani, *Robust Power System Frequency Control*, 2nd ed. Cham, Switzerland: Springer, 2014, doi: 10.1007/978-3-319-07278-4.
[4] P. Tielens and D. Van Hertem, "The relevance of inertia in power systems," *Renew. Sustain. Energy Rev.*, vol. 55, pp. 999–1009, 2016, doi: 10.1016/j.rser.2015.11.016.
[5] A. Ulbig, T. S. Borsche, and G. Andersson, "Impact of low rotational inertia on power system stability and operation," *IFAC Proc. Vol.*, vol. 47, no. 3, pp. 7290–7297, 2014, doi: 10.3182/20140824-6-ZA-1003.02615.

[6] J. Marcos, L. Marroyo, E. Lorenzo, D. Alvira, and E. Izco, "Power output fluctuations in large scale PV plants: One year observations with one second resolution and a derived analytic model," *Prog. Photovolt.: Res. Appl.*, vol. 19, no. 2, pp. 218–227, 2011, doi: 10.1002/pip.1016.

[7] I. A. Samuel, J. Katende, S. A. Daramola, and A. A. Awelewa, "Review of system collapse incidences on the 330-kV Nigerian National Grid," *Int. J. Eng. Sci. Invention*, vol. 3, no. 4, pp. 55–59, 2014.

[8] W. Tan, "Unified tuning of PID load frequency controller for power systems via IMC," *IEEE Trans. Power Syst.*, vol. 25, no. 1, pp. 341–350, 2010, doi: 10.1109/TPWRS.2009.2036463.

[9] Z. Li, "Review of PID control design and tuning methods," *J. Phys.: Conf. Ser.*, vol. 2649, no. 1, Art. no. 012009, 2023, doi: 10.1088/1742-6596/2649/1/012009.

[10] D. H. Wolpert and W. G. Macready, "No free lunch theorems for optimization," *IEEE Trans. Evol. Comput.*, vol. 1, no. 1, pp. 67–82, 1997, doi: 10.1109/4235.585893.

[11] T. Prakash, P. P. Singh, V. P. Singh, and S. N. Singh, "A novel brown-bear optimization algorithm for solving economic dispatch problem," in *Advanced Control & Optimization Paradigms for Energy System Operation and Management*. Gistrup, Denmark: River Publishers, 2023, pp. 137–164, doi: 10.1201/9781003337003-6.

[12] Q. Askari, I. Younas, and M. Saeed, "Political optimizer: A novel socio-inspired meta-heuristic for global optimization," *Knowl.-Based Syst.*, vol. 195, Art. no. 105709, 2020, doi: 10.1016/j.knosys.2020.105709.

[13] S. Mirjalili, S. M. Mirjalili, and A. Lewis, "Grey wolf optimizer," *Adv. Eng. Softw.*, vol. 69, pp. 46–61, 2014, doi: 10.1016/j.advengsoft.2013.12.007.

[14] Ibraheem, P. Kumar, and D. P. Kothari, "Recent philosophies of automatic generation control strategies in power systems," *IEEE Trans. Power Syst.*, vol. 20, no. 1, pp. 346–357, 2005, doi: 10.1109/TPWRS.2004.840438.

[15] H. Shayeghi, H. A. Shayanfar, and A. Jalili, "Load frequency control strategies: A state-of-the-art survey for the researcher," *Energy Convers. Manage.*, vol. 50, no. 2, pp. 344–353, 2009, doi: 10.1016/j.enconman.2008.09.014.

[16] A. Pappachen and A. P. Fathima, "Critical research areas on load frequency control issues in a deregulated power system: A state-of-the-art-of-review," *Renew. Sustain. Energy Rev.*, vol. 72, pp. 163–177, 2017, doi: 10.1016/j.rser.2017.01.053.

[17] M. M. Gulzar, D. Sibtain, M. Alqahtani, F. Alismail, and M. Khalid, "Load frequency control progress: A comprehensive review on recent development and challenges of modern power systems," *Energy Strategy Rev.*, vol. 57, Art. no. 101604, 2025, doi: 10.1016/j.esr.2024.101604.

[18] A. Abbasi, S. M. S. Hussain, M. M. Gulzar, and M. Khalid, "LFC strategies for future power grids: A survey on intelligent, data-driven, and resilient techniques," *Energy Convers. Manage.: X*, Art. no. 101461, 2025, doi: 10.1016/j.ecmx.2025.101461.

[19] S. G. Moghaddam, A. A. Bagheri, and R. Sedaghati, "Load-frequency control in a two-area power system using the fuzzy-PID method," *ECTI Trans. Electr. Eng., Electron., Commun.*, vol. 21, no. 1, Art. no. 248665, 2023, doi: 10.37936/ecti-eec.2023211.248665.

[20] J. H. Holland, *Adaptation in Natural and Artificial Systems*. Ann Arbor, MI, USA: Univ. Michigan Press, 1975.

[21] J. Kennedy and R. Eberhart, "Particle swarm optimization," in *Proc. IEEE Int. Conf. Neural Netw. (ICNN'95)*, Perth, WA, Australia, 1995, vol. 4, pp. 1942–1948, doi: 10.1109/ICNN.1995.488968.

[22] D. Guha, P. K. Roy, and S. Banerjee, "Load frequency control of interconnected power system using grey wolf optimization," *Swarm Evol. Comput.*, vol. 27, pp. 97–115, 2016, doi: 10.1016/j.swevo.2015.10.004.

[23] N. A. Orka, S. S. Muhaimin, M. N. S. Shahi, and A. Ahmed, "An enhanced gradient based optimized controller for load frequency control of a two-area automatic generation control system," in Engineering Applications of Modern Metaheuristics. Cham, Switzerland: Springer, 2022, pp. 79–107, doi: 10.1007/978-3-031-16832-1_5.

[24] A. B. Wazir, A. Althobiti, A. A. Alhussainy, S. Alghamdi, M. Vellingiri, T. Palaniswamy, and M. Rawa, "A comparative study of load frequency regulation for multi-area interconnected grids using integral controller," *Sustainability*, vol. 16, no. 9, Art. no. 3808, 2024, doi: 10.3390/su16093808.

[25] R. K. Sahu, S. Panda, and U. K. Rout, "DE optimized parallel 2-DOF PID controller for load frequency control of power system with governor dead-band nonlinearity," *Int. J. Electr. Power Energy Syst.*, vol. 49, pp. 19–33, 2013, doi: 10.1016/j.ijepes.2012.12.009.

[26] M. N. S. Shahi, N. A. Orka, and A. Ahmed, "2DOF-PID-TD: A new hybrid control approach of load frequency control in an interconnected thermal-hydro power system," *Heliyon*, vol. 10, no. 17, Art. no. e36753, 2024, doi: 10.1016/j.heliyon.2024.e36753.